RSC Advances

PAPER

Cite this: *RSC Adv.*, 2015, **5**, 72482

Synthesis, biological activity and structural study of new benzotriazole-based protein kinase CK2 inhibitors†

R. Swider,[ab] M. Masłyk,[ab] J. M. Zapico,[a] C. Coderch,[a] R. Panchuk,[c] N. Skorokhyd,[c] A. Schnitzler,[d] K. Niefind,[d] B. de Pascual-Teresa*[a] and A. Ramos*[a]

Received 23rd June 2015
Accepted 17th August 2015

DOI: 10.1039/c5ra12114k

www.rsc.org/advances

A new series of 4,5,6,7-tetrabromobenzotriazole (TBB) derivatives was synthesized and characterized as CK2 inhibitors. They were readily synthesized using a click chemistry approach based on a Cu(I)-catalyzed azide-alkyne 1,3-dipolar cycloaddition (CuAAC). Some of the synthesized compounds present interesting inhibitory activities using an *in vitro* assay, with K_i values in the low micro molar range and a high degree of selectivity against a panel of 24 kinases. Selected compounds were tested for their antiproliferative effect on several cancer cell lines, and for their proapoptotic activity towards human Jurkat T-leukemia and MCF-7 breast adenocarcinoma cells, showing that they can be proposed as promising anticancer agents. Docking studies as well as crystallographic analysis allowed us to identify ligand–CK2 interactions that account for the molecular recognition process, and can help to further optimize this family of compounds as CK2 inhibitors.

Introduction

Protein kinase CK2 (formerly known as casein kinase 2) is a ubiquitously expressed, constitutively active serine/threonine protein kinase that participates in the regulation of multiple signaling pathways of proliferation, differentiation and survival, including DNA damage response, PI3K/Akt pathway, Wnt cascade and NF-κB transcription.[1–3] This enzyme is composed of two catalytic subunits, CK2α, CK2α′ and a dimer of a regulatory subunit CK2β. A number of experimental data indicated the importance of all CK2 subunits in cell life. Knockout of CK2β resulted in embryonic lethality, while knockout of CK2α′ caused defects in spermatogenesis in mice.[4,5] Furthermore, genetic studies provided evidence of the need of both catalytic subunits in cell life. Knockout of CK2α and α′ resulted in cell lethality in yeast.[6,7] Expression of CK2 is highly elevated in tumor cells where it protects cells from apoptosis. Accordingly, inhibition of CK2 is known to induce programmed cell death, making it a promising target for cancer therapy.[8]

Up to date many compounds have been reported as potent CK2 inhibitors.[9–16] TBB,[17] DMAT,[18,19] and ellagic acid[20] with sub-micromolar K_i values are representatives of ATP-competitive inhibitors (Fig. 1). More recently, the success of CX-4945 (Fig. 1) as an orally bioavailable selective, ATP competitive CK2 inhibitor ($IC_{50} = 1$ nM) constituted a major progress in this field.[21–23]

We have recently presented our preliminary results on the search of new TBB derivatives designed to interact simultaneously with the adenosine binding pocket and the substrate-binding site of the enzyme.[24]

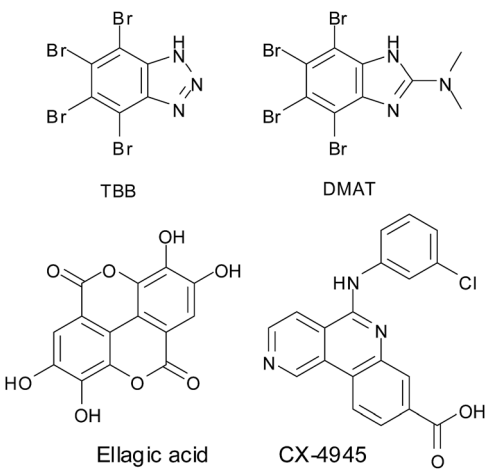

Fig. 1 Examples of ATP-competitive inhibitors of CK2.

[a]*Departamento de Química y Bioquímica, Facultad de Farmacia, Universidad CEU San Pablo, 28668 Boadilla del Monte, Madrid, Spain. E-mail: aramgon@ceu.es; bpaster@ceu.es*

[b]*Department of Molecular Biology, Faculty of Biotechnology and Environmental Sciences, The John Paul II Catholic University of Lublin, 20-718, Lublin, Poland*

[c]*Institute of Cell Biology, NAS of Ukraine, Drahomanov Str. 14/16, 79005 Lviv, Ukraine*

[d]*Department of Chemistry, Institute of Biochemistry, University of Cologne, Otto Fischer-Str. 12-14, D-50674 Cologne, Germany*

† Electronic supplementary information (ESI) available: ^{1}H and ^{13}C NMR spectra of **9**, **10**, **14–17**, **20–22**; First Docking studies. See DOI: 10.1039/c5ra12114k

We found that the introduction of a 1-(4-aminobutyl)-1*H*-1,2,3-triazol-4-yl chain on the N^2-atom of TBB gave a compound with a promising inhibitory activity of CK2. Here we report the experimental details of the synthesis of this compound and a series of N^1- and N^2- substituted analogs. The inhibitory activity of the synthesized compounds was tested using a standard kinase assay and the selectivity of selected compounds against a panel of 24 enzymes was determined. Antiproliferative activity of these compounds was tested against three different cancer cell lines, and a study of the proapoptotic activity was performed using annexin V/PI double staining assay and DNA hypercondensation analysis, making use of DAPI (4′,6-diamidino-2-phenylindole) staining protocol. In order to rationalize the biological activity, a structural characterization of the CK2-inhibitor complexes was performed using a combination of crystallographic and docking techniques.

Results

Chemistry

TBB, a small molecule provided of high selectivity towards CK2, was chosen as scaffold for the design of our compounds, and a click chemistry approach based on the copper(I)-catalyzed azide alkyne cycloaddition (CuAAc) reaction between a series of azides and alkynes was used to synthesize most of them.

Azides **1–3** were synthesized by reaction of the corresponding commercially available bromide with sodium azide in DMF at 60–70 °C. They were purified by column chromatography and used as substrates in the cycloaddition reaction with alkynes. TBB was synthesized according to the method described previously.[25] Reaction of TBB with 4-bromo-1-butyne in the presence of K_2CO_3 gave a mixture of the N^1-alkylated and N^2-alkylated compounds **4** and **5** (Scheme 1), which were successfully isolated and purified by column chromatography on alumina. In the reaction of **TBB** with *tert*-butyl 2-bromoethylcarbamate, the formation of two isomers was also observed by TLC (thin layer chromatography), but only isomer **6** could be isolated (Scheme 1).

Azides **1–3** were connected to alkynes **4** and **5** using a CuAAc reaction to obtain triazoles **7**, **8**, **11–13** (Scheme 1). We used a Cu(II)/ascorbic acid system as catalyst, and DMF as solvent. Triazoles were obtained with moderate to good yields (from 60% to 99%) after 24–48 hours at room temperature. The reaction was completely regioselective giving 1,4-disubstituted triazoles exclusively, which were purified by column chromatography or by crystallization. Finally, deprotection of the Boc-protected amino group in **6–8**, **11–13** by reaction with TFA (trifluoroacetic acid) in DCM (dichloromethane) provided amines **9**, **10**, **14–17** (Scheme 1).

In order to assess the influence of the triazole connecting ring, compounds **19–22**, where this ring was substituted by an amide, were synthesized as depicted in Scheme 2. In compound **20**, the terminal amino group was replaced by a hydroxyl group, and in **21–22** by a carboxylic acid. Amide **18** was obtained by direct condensation of amine **17** with 3-(*tert*-butoxycarbonylamino)acetic acid in the presence of HOBT (hydroxybenzotriazole), HBTU ((2-(1*H*-benzotriazol-1-yl)-1,1,3,3-tetramethyluroniumhexafluorophosphate) and NMM (*N*-methylmorpholine) as activating agents. Removal of the Boc-protecting group in **18** by treatment with TFA/DCM gave compound **19**. Finally, coupling of **17** with γ-butyrolactone, succinic anhydride or glutaric anhydride provided **20**, **21** and **22** respectively (Scheme 2).

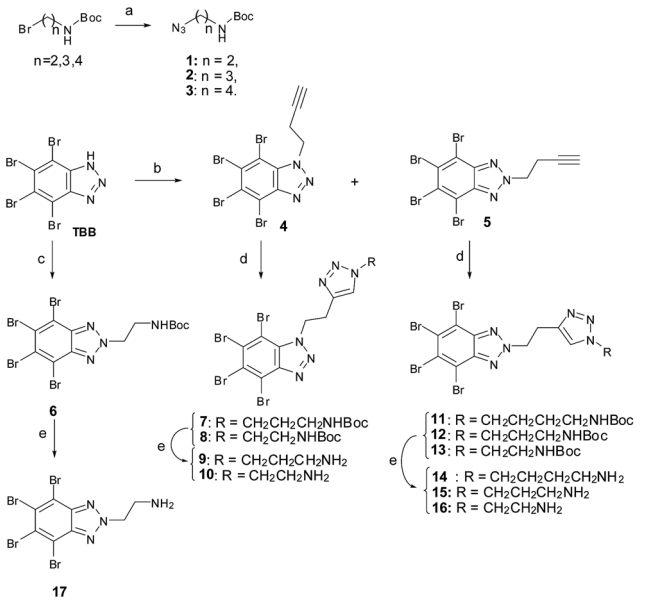

Scheme 1 Synthesis of compounds **1–17**. Reagents and conditions: (a) NaN_3, DMF, 60–70 °C; (b) 4-bromo-1-butyne, K_2CO_3, acetone, 60 °C; (c) *tert*-butyl 2-bromoethylcarbamate, acetone, K_2CO_3, 60 °C; (d) N_3R, $CuSO_4 \cdot 5H_2O$, sodium ascorbate, DMF; (e) DCM, TFA.

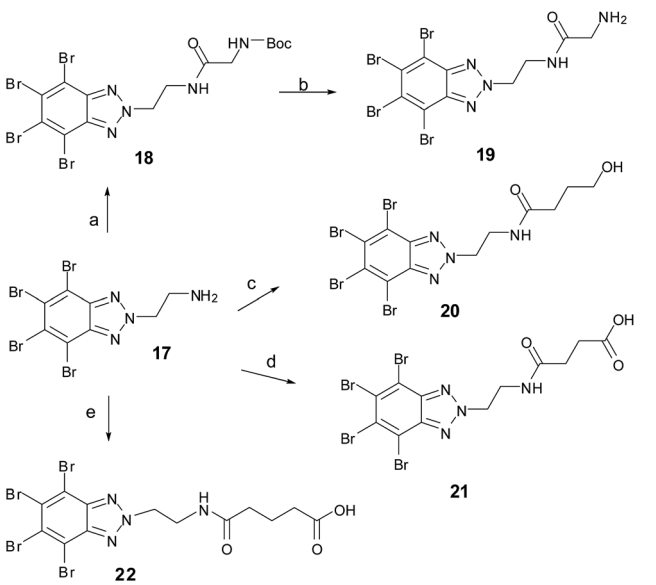

Scheme 2 Synthesis of TBB derivatives **18–22**; Reagents and conditions: (a) 3-(*tert*-butoxycarbonylamino)acetic acid, HOBT, HBTU, NMM, r.t.; (b) TFA in DCM, r.t.; (c) γ-butyrolactone, toluene, reflux; (d) succinic anhydride, EtOH, reflux; (e) glutaric anhydride, EtOH.

Biology

Inhibitory activity. *In vitro* inhibitory activity of the synthesized compounds was determined using a radiometric assay. The remaining CK2 activity values for both catalytic subunits CK2α and CK2α′ and the K_i for the most active compounds are presented in Table 1.

Selectivity profiles. To assess the selectivity of **10**, **14** and **16**, these compounds were profiled at 10 μM concentration on a panel of 24 kinases, using the KINOME*scan*™ methodology (DiscoveRx). KINOME*scan*™ is based on a competition binding assay that quantitatively measures the ability of a compound to compete with an immobilized ligand which is bound to the active site of the DNA tagged kinase. The ability of the test compound to compete with the immobilized ligand is measured *via* quantitative PCR of the DNA tag.[26] Results are collected in Table 2.

Table 2 KINOME*scan*™ (DiscoveRx Corporation) profile of a panel of 24 kinases for inhibitors **10**, **14** and **16** at 10 μM[a]

	10	**14**	**16**
Target	% control 10 μM	% control 10 μM	% control 10 μM
AKT1	100	100	100
AURKA	100	94	100
CAMK1	69	89	89
CDK2	90	100	100
CLK2	14	74	5.3
CK1	54	94	47
CK2α	0.37	0.78	0.24
DRAK1	58	81	75
DYRK1A	25	61	16
ERK8	54	92	91
HIPK2	1.4	38	0.4
IKK-α	74	100	51
MAPKAPK2	84	84	88
MKNK2	48	73	40
MLK1	88	100	100
PDGFRB	77	81	87
PDPK1	85	94	100
PIM1	2.3	37	3.4
PKAC-α	98	100	100
PRKCK	78	92	76
PRKD1	84	98	96
PRKG1	56	55	88
SRC	93	95	100
TRKA	80	89	77

[a] % control calculation: [(test compound signal − positive control signal)/(negative control signal − positive control signal)] × 100.

Cytotoxic activity against cancer cells

We selected compounds **10**, **14** and **16** for further *in vitro* studies on the following tumor cell lines: human leukemia Jurkat T-cell line, murine leukemia L1210 cell line, estrogen resistant human breast adenocarcinoma MDA-MB 231 cell line, and estrogen sensitive human breast adenocarcinoma MCF-7 cell line.

LC_{50} index was used to express the concentration of drug which kills 50% of the cells in comparison to control culture, and the results are collected in Table 3. The three compounds killed cancer cells in a dose-dependent mode on both carcinoma and leukemia cells, as can be seen in Fig. 2.

The most significant apoptotic changes in the nuclei of MCF-7 cells were observed under treatment with LC_{75} of the tested compounds, while for LC_{50} such effect was not so relevant. Doxorubicin (Dx), a well-known anticancer drug widely used in the clinic, was used as positive control.[27,28] Massive vacuolization of cell cytoplasm was observed under treatment of MCF-7 cells with the three selected compounds, thus confirming annexin V/PI data obtained for these compounds.

Apoptosis/necrosis assay. Cytomorphologic studies were performed in order to identify the mechanism (apoptotic or necrotic) by which these CK2 inhibitors induce the death of the target cells. Phosphatidylserine translocation to the external layer of the cell membrane of dying cells measured by the annexin V test is one of the earliest hallmarks of apoptosis.[29]

Table 1 *In vitro* activity profile and lipophilicity data for the synthesized compounds toward CK2α and CK2α′

	K_i [μM]		Remaining CK2 activity after treatment with a 10 μM solution of selected compounds [%]			
Comp.	CK2α′	CK2α	CK2α′	CK2α	*c* log $D_{7.4}$[a]	*c* log *P*[a]
9	2.06 ± 0.29	1.04 ± 0.13	37.0 ± 0.1	29.9 ± 0.2	1.54	4.10
10	1.58 ± 0.18	0.8 ± 0.2	31.4 ± 0.1	23.1 ± 1.0	1.90	4.04
14	7 ± 2	3.35 ± 0.88	48.4 ± 0.4	44.5 ± 1.2	1.95	4.46
15	2.29 ± 0.28	0.95 ± 0.11	28.0 ± 0.1	26 ± 7	1.35	3.91
16	1.26 ± 0.21	0.76 ± 0.18	37.7 ± 0.1	20.1 ± 0.6	1.71	3.85
17	2.56 ± 0.22	1.91 ± 0.25	40.1 ± 0.1	32 ± 5	1.49	3.59
19	3.52 ± 0.37	1.63 ± 0.14	42.4 ± 0.1	38.4 ± 0.1	1.66	2.47
20	nd	nd	52 ± 3	52.1 ± 0.2	3.18	3.18
21	nd	nd	44.2 ± 0.9	45.5 ± 1.1	0.23	3.24
22	nd	nd	49 ± 2	47.2 ± 1.4	0.60	3.71

[a] Calculator plugins were used for *c* log *P* and *c* log *D* values, Marvin 5.9.1, 2012, ChemAxon http://www.chemaxon.com.

Table 3 LC_{50} (μM) cytotoxic activity of compounds **10**, **14** and **16**

Compound	Jurkat T-cells	L1210	MDA-MD-231	MCF-7
10	14.2 ± 1.4	20.7 ± 1.4	17.4 ± 0.9	17 ± 2
14	8.7 ± 0.5	11.42 ± 0.04	9.7 ± 0.4	9.0 ± 0.7
16	7.9 ± 0.3	14.3 ± 0.6	14 ± 1	11.6 ± 0.8

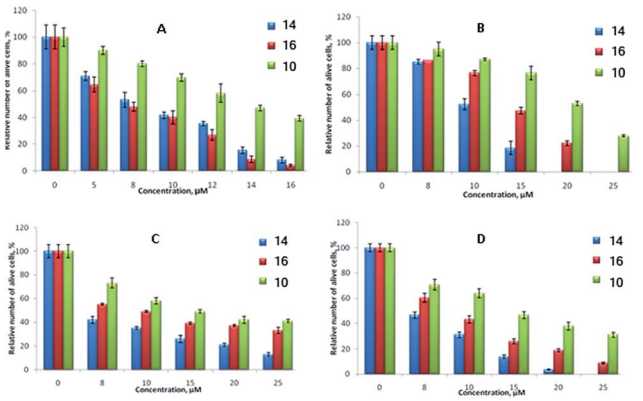

Fig. 2 Comparison of cytotoxic activity of **10**, **14**, and **16** toward several cancer cell lines. (A) leukemia Jurkat T-cell line, (B) murine leukemia L1210 cell line, (C) breast adenocarcinoma MDA-MB 231 cell line, (D) breast adenocarcinoma MCF-7 cell line.

Propidium iodide (PI) is a DNA targeting dye, which detects only necrotic cells, since alive cells use membrane pumps to remove it out to the extracellular medium. Supravital double staining of Jurkat T-leukemia cells, treated with LC_{50} concentrations of **10**, **14** and **16** and with FITC-conjugated annexin V and PI revealed that these compounds induce apoptosis in the cells, though after 24 h of treatment we observed an increase in the number of late apoptotic (*e.g.* secondary necrotic) cells (Fig. 3).

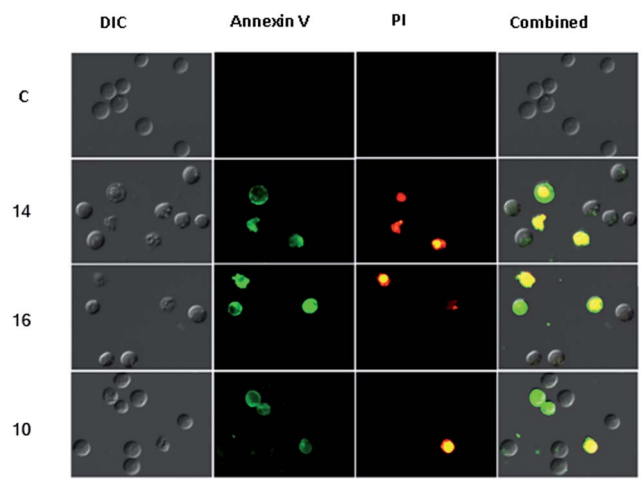

Fig. 3 Proapoptotic activity of CK2 inhibitors toward Jurkat T-leukemia cells. Compounds were used in the following concentrations: **14** – 10 μM, **16** – 8 μM, **10** – 14 μM; C – control, DIC – differential interference contrast.

Chromatin condensation is another important characteristic of apoptosis. It can be easily measured by means of DNA-intercalating dyes, such as DAPI. We found that the three tested compounds caused the development of chromatin hyper-condensation in MCF-7 cells, thus leading to apoptosis in carcinoma cells (Fig. 4).

Structural study. In order to rationalize the biological results discussed above, several docking studies were performed with the selected compounds **10**, **14** and **16**. For the first docking (ESI†) the initial choice of the crystal structure was based mainly on the conformation of His160 which is important for the binding of the ribose of the GTP as can be seen in structure of CK2 in complex with AMP-PNP (a non-hydrolysable ATP-analogue) as starting geometry (PDB code 3NSZ). In this crystal structure there is a double occupancy for the side chain of His160: one oriented towards the ribose of AMP-PNP and the other facing bulk solvent. The latter conformation was selected for the docking studies as it gives a less hindered binding site. In order to assess this first theoretical study using the 3NSZ crystal structure, and confirm the proposed binding mode, a crystallographic analysis was performed for **14** (Fig. 5). To investigate the enzyme/inhibitor interaction eliminating the possibility of crystal packing artifacts, human $CK2\alpha^{1-335}$/**14** complex was determined by two different crystal symmetries and crystallization methods. A tetragonal crystal form was grown by co-crystallization while a monoclinic form of the crystalline inhibitor/enzyme complex was generated by ligand exchange *via* soaking (See Table 4 in Experimental section for X-ray data collection and refinement statistics). In both cases, the TBB core occupies the same space in the ATP-binding pocket and is well defined by electron density and form halogen bonds to electron-rich Lewis bases of the protein *via* each of the four bromo substituents.[30] By contrast, the triazole-containing side chain is more flexible, but at least partially visible. In the complex obtained by co-crystallization, the triazole ring coordinates Asp120 and the terminal amine is oriented outside the pocket. However, a different orientation of the side chain of **14** was observed when the soaking method was applied. In this case, the chain is located under the phosphate anchor loop with the terminal amine directed towards Tyr50 (Fig. 5). The overall structure of the protein obtained with the two crystallization methods was the same, only slight differences were found in the phosphate anchor loop obtained

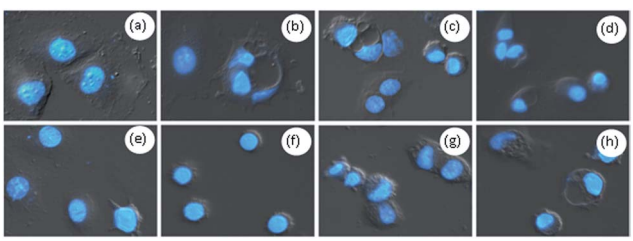

Fig. 4 Influence of CK2 inhibitors **10**, **14** and **16** on DNA hyper-condensation in human breast adenocarcinoma MCF-7 cells. DAPI staining, 24 h after treatment (a) control; (b) **Dx**, 0.5 μM; (c) **14**, 10 μM; (d) **14**, 15 μM; (e) **16**, 15 μM; (f) **16**, 20 μM; (g) **10**, 20 μM; (h) **10**, 25 μM.

through soaking. In this structure, this loop appears slightly more opened than the one obtained through co-crystallization, because the amine moiety of the ligand was lodged under it, forcing an induced fit of the protein. The soaking method gave results, which are in accordance with the docking predictions. In both cases the side chain of **14** is oriented below the phosphate anchor loop, although some differences are observed. Thus, docking studies predict that the amino group at the end of the chain coordinates Asp156, while the crystal structure shows that this group is oriented toward Tyr50.

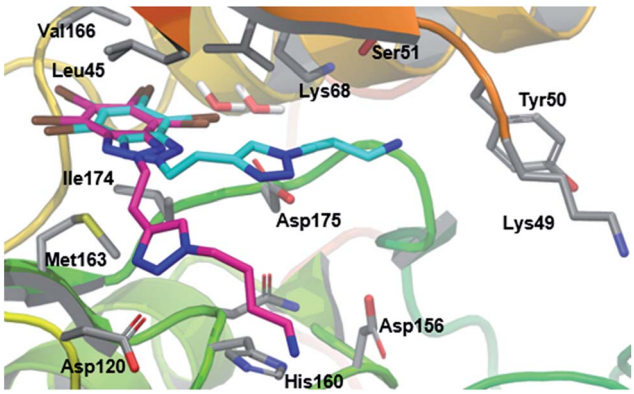

Fig. 5 Crystal structures of human CK2α^{1-335} complexes with compound **14**. Complexes of CK2α^{1-335} and the inhibitor were generated by pre-incubation/co-crystallization and ligand exchange by soaking. The protein structure is represented as rainbow cartoons and the main amino acid side chains that interact with the ligands are shown in grey sticks. Carbons in ligand **14** in the complex with CK2α are colored pink and cyan for co-crystallization and soaking methods, respectively.

The two conformations found in the crystal structures suggested a high flexibility of the ligands. Therefore, to further assess our previous docking studies, they were repeated using near-end versions of the two CK2 crystal structures in complex with compound **14** differing marginally from the final depositions (5CQU, 5CQW) due to minor adaptations in the course of the reviewing process. The most commonly used docking protocol considers the protein to be rigid and the ligand flexible, so the results depend on the protein conformation and the amino acid conformation of the binding site. In addition, for docking purposes water molecules found in the crystal structures are usually removed and the solvation of the whole system is considered implicitly using the dielectric effect of water. Therefore slight differences in the proteins will give different docking solutions.

The docking of compounds **10**, **14** and **16** on co-crystallization-issued structure (PDB code 4BXA) rendered a common pose for the TBB moiety within the ATP binding site in CK2. The common TBB core established van der Waals interactions with the side chains of Val53, Val66, Ile95, Phe113, Met163 and Ile174 within the adenine-binding site, just as in our first docking studies.

Table 4 X-ray data collection and refinement statistics

	Complex by ligand exchange *via* soaking (PDB 5CQU)	Complex by co-crystallization (PDB 5CQW)
Data collection		
Temperature [K]	100	100
Wavelength [Å]	1.0000	1.0000
Space group	$P2_1$ (monoclinic)	$P4_32_12$ (tetragonal)
Cell dimensions		
a, *b*, *c* [Å]	58.48, 46.89, 63.46	127.09, 127.09, 126.84
α, β, γ [°]	90.00, 111.56, 90.00	90.00, 90.00, 90.00
Resolution [Å]	35.52–2.35 (2.48–2.35)[a]	44.93–2.65 (2.79–2.65)[a]
R_{sym} [%]	12.1 (37.2)[a]	14.4 (117.3)[a]
Signal to noise ratio ($I/\sigma I$)	13.4 (2.2)[a]	13.1 (2.0)[a]
No. of unique reflections	13 506 (1936)[a]	30 832 (4407)[a]
Completeness [%]	99.7 (98.3)[a]	100 (100.0)[a]
Multiplicity	3.3 (2.7)[a]	7.4 (4.5)[a]
B-factor from Wilson plot [Å^2]	38.88	50.35
Refinement		
No. of refl. in working set/test set	12 843/668	29 212/1547
R_{work}/R_{free} [%]	19.6/25.1	18.8/23.0
No. of atoms		
Protein	2779	5594
Ligand/ion	53	131
Water	118	154
R.m.s deviations		
Bond lengths [Å]	0.002	0.002
Bond angles [°]	0.51	0.58
Ramachandran favored [%]	97.0	97.0
Ramachandran outliers [%]	0.0	0.0
Average B-factor [Å^2]	46.80	57.90

[a] Value in parentheses are for highest resolution shell.

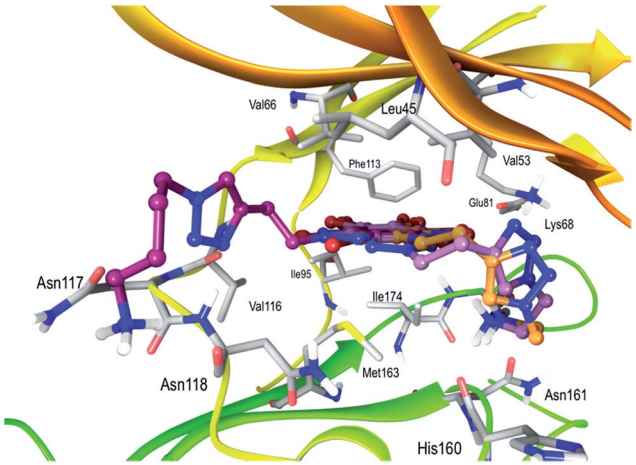

Fig. 6 Maestro representation of the structure of human CK2α represented as rainbow-colored cartoons in complex with compounds **10**, **14** and **16** represented respectively as light orange, dark magenta and pink balls and sticks. For the sake of clarity only polar hydrogens are displayed; and only the side chains of the amino acids that interact with the compounds are represented as grey sticks. Due to the image orientation the side chain of Asp175 lies hidden behind the amine end of compounds **10** and **16** with which it establishes a hydrogen bond, while the amine end of **14** protrudes toward the outside of the protein interacting with Asn117.

Interestingly, the side chain containing the amine drives the orientation of the compounds within the lining of the ATP-binding site. Compounds **10** and **16** adopt a pose that orients the amine end towards the magnesium-binding site of the enzyme where it establishes hydrogen-bonding interactions with the backbone oxygen of His160 and the side chains of Asn161 and Asp175, in a similar orientation as crystal structure 4BXB. Interestingly, compound **14** did not adopt that binding pose and protruded the amine end towards the exterior of the binding site just as in the crystal structure 4BXA (Fig. 6). When the dockings where repeated with the soaking-issued structure (PDB code 4BXB), compound **16** reproduced the docked pose of the previous docking with the TBB lodged deep in the binding pocket and the amine end oriented towards the magnesium-binding site, whereas, while maintaining the same binding pose for the TBB moiety as compound **16**, compound **10** protruded the amine towards the exterior of the binding site as did compound **14** in the previous docking. As for compound **14**, the docking pose obtained with this protein was not able to reproduce the bound conformation seen in any of the crystal structures, mainly due to the previously described characteristics of the protocol (ESI, Fig. S2†). Summarizing, we see mainly two possible interaction patterns that are in line with the two possible conformations found in the crystal structures of compound **14** in complex with CK2.

Discussion

Strategies based on the use of halogenated benzimidazoles and benzotriazoles as inhibitors of CK2 have been developed for more than 20 years.[31] The progress in the study of the relationship between structural aspects and biological activity has led to new and more potent inhibitors. On the other hand, crystallographic and computational studies have led to a better understanding of the mode of action of these inhibitors.

The compounds presented in this work were designed based on TBB, which has already been described as a potent and selective inhibitor of CK2.[32] In order to evaluate the drug-like properties of the synthesized compounds, estimated log *P* and log *D* (at pH 7.4) values were calculated and are presented in Table 1. All of them present values within the range accepted for an orally active drug.

"Clicked" compounds **9**, **10**, **15** and **16** had the highest inhibitory activities, with K_i values in the low micromolar range. Among them, **10** and **16**, with a linker of two carbon atoms between the imidazole ring and the terminal amino group were the most active compounds (0.78 and 0.76 μM in CK2α respectively). Compounds **9** and **15**, with one more carbon atom at this position presented slightly higher values of K_i, and compound **14**, with a four carbon atom linker at this position was found to be 4.5 less active than **10** and **16**. The change of the basic side chain from N2 to N1 in the triazole ring resulted in negligible differences in the inhibition constant values, as can be seen by comparing compounds **15** and **16** with their isomers **9** and **10**.

Amine **17**, where a short aminoethyl group is attached to the TBB moiety was also active at micromolar concentration. Compounds **19–22** where the triazole ring was substituted by an amide linker and different polar groups (NH_2, OH or COOH) were introduced at the end of the side chain did not improved the activity of the "clicked" compounds, and their K_i values were not calculated.

Although the most potent compounds of our "clicked" series are less active than TBB, their K_i values are comparable to the values described for other CK2 inhibitors, such as MNA (1,8-dihydroxy-4-nitroanthraquinone) (K_i = 0.78 μM) and Apigenin (K_i = 0.74 μM). Based on these interesting results, we studied the selectivity of **10**, **14** and **16** against a panel of 24 kinases. As shown in Table 3, compounds **10** and **16** exhibited binding competition of the immobilized ligand of 95% or more to only CK2α, HIPK2 and PIM1 at the concentration of 10 μM. This selectivity profile is common to other TBB and DMAT-derived compounds.[33] Moreover, the less active compound **14** resulted more selective than **10** and **16**.

We attempted to confirm the binding affinity of these compounds through the measurement of the dissociation constant (K_D) to CK2. Sub-300 nM K_D against CK2α was obtained for **10**, **14** and **16** (63, 290 and 70 nM, respectively), an affinity higher than the one obtained for TBB (K_D = 800 nM) under the same conditions.

Cell line experiments were undertaken with compounds **10**, **14** and **16**. We selected **10** and **16** because they were the most active compounds in isolated enzyme experiments, and **14** because of its selectivity against all the tested enzymes.

It was observed that the three compounds inhibit cancer cell growth at micro-molar concentration and in a dose-dependent mode (Fig. 2). They made no difference between estrogen-sensitive and estrogen-resistant breast cancer models *in vitro*, which indicates that CK2 inhibitors kill tumor cells of different

origin with equal efficiency. This could be relevant when moving to *in vivo* studies.

Compound **14**, in spite of being the less active in isolated enzyme, displayed the highest cytotoxic activity on both carcinoma and leukemia cells (Table 3). Compound **16** showed similar cytotoxic activity, while its isomer **10**, despite having almost identical K_i values toward CK2 than **16**, showed a 50% decrease of activity. Worse permeability properties of the N^1-substituted derivatives could be responsible for the observed differences.

Some interesting conclusions can be drawn when comparing the cytotoxic effect of the tested compounds with the values described for TBB. Thus, the treatment of Jurkat cells with 10 μM TBB resulted in a reduction of cell viability to 60%,[33] a lower effect than the one exerted by compounds **14** and **16** in these cells (reduction of viability to 40 at 10 μM). Moreover, the viability of MCF-7 cells and MDA-MB-231 cells treated with 100 μM TBB was reduced only to 90%,[34] whereas the average value of LC_{50} for the examined compounds towards these cell lines is about 13 μM (Fig. 2). Taking into account that TBB displays higher inhibition of CK2 (K_i = 0.4 μM) than our compounds, the obtained results indicate that the introduction of a basic side chain in TBB, in spite of producing a decrease of inhibition of the isolated enzyme, maintains or even improves the cytotoxic activity. This could be explained by an improvement of the permeability compared to the un-substituted compound.

It has been proposed that dual inhibitors of protein kinase CK2 and PIM-1 are tools particularly valuable to induce apoptosis of cancer cells.[12] Study of cell death mechanisms induced by the novel CK2 inhibitors **10**, **14** and **16** using annexin V/PI and DAPI staining revealed the appearance of typical hallmarks of apoptosis (phosphatidylserine externalization and nuclear chromatine hypercondensation) in leukemia and carcinoma cells. Again, the position of the basic side chain in the molecule has an effect on the results. Compound **16** produced a pro-apoptotic activity 50% higher than its isomer **10**, a result that correlates closely with the cytotoxicity studies for these inhibitors (see Fig. 2).

The binding mode of the synthesized compounds was predicted using docking techniques by using Maestro Suite from Schrodinger with Extra Precision mode. This approach led to slight differences in comparison to the crystallographic results but, overall, we have found two possible binding modes in line with the crystallographic results. There are two water molecules in the active site that are considered as highly relevant, since they have been found in almost all CK2 crystallographic structures solved to date.[32,35] These two water molecules were also found in our experimental complexes. Finally, if we compare the crystallographic structure of CK2α/**14** complex with other CK2–ligand complexes solved by X-ray crystallography, we can observe some interesting relationships. The crystal structure of TBB in complex with (maize) CK2α (PDB code: 1J91) revealed that the ligand is located rather deeply within the ATP binding site, and much deeper than 4,5,6,7-tetrabromobenzimidazole in complex with CK2 (PDB code: 2OXY). This difference can be explained because the tetrabromobenzotriazole 5-ring – unlike the tetrabromobenzimidazole 5-ring – is acidic and negatively charged at physiological pH,[32] so that the whole molecule is attracted to a well-described positively charged area close to the conserved Lys68 side chain.[36] In contrast, the TBB-core of **14** is substituted at N^2-position, which prevents deprotonation and the subsequent formation of a negative charge. In this sense, compound **14** is more similar to substituted tetrabromobenzimidazole derivatives, which explains the orientation that we found for the TBB core of **14** in complex with CK2. Interestingly, depending on the nature of the substituent of the imidazole ring, the tetrabromobenzimidazole derivatives will adopt different orientations. If the substituent is small such as in 4,5,6,7-tetrabromo-*N*,*N*-dimethyl-1*H*-benzimidazol-2-amine (PDBID: 1ZOE) or even non aliphatic such as in 4,5,6,7-tetrabromo-1*H*,3*H*-benzimidazol-2-one and 4,5,6,7-tetrabromo-1*H*,3*H*-benzimidazol-2-thione (PDBID: 2OXD and 2OXX), an orientation of the ligand similar to the native tetrabromobenzimidazole (PDBID: 2OXY) is found.[19,36] The same happens with an additional acidic substitution such as in the case of the 2-dimethylamino-4,5,6,7-tetrabromobenzoimidazol-1yl-acetic acid (PDBID: 3KXH) or the 4,5,6,7-tetrabromo-1-carboxymethylbenzimidazole (PDBID: 3PVG).[35] When the tetrabromobenzimidazole derivatives present an aliphatic substitution they adopt a somewhat flexible or even ambiguous orientation within the CK2α subunit. That flexibility depends greatly on the nature of the substituent that will orient the ligand depending on the different interactions. Therefore, the TBB moiety of compound **14** adopts an orientation that only occurs with aliphatic substitutions, namely in case of *N*-(6-oxohexyl)-2-(4,5,6,7-tetrabromo-1*H*-benzimidazol-1-yl)acetamide (PDBID: 4FBX), *N*-methyl-2-[(4,5,6,7-tetrabromo-1-methyl-1*H*-benzimidazol-2-yl)sulfanyl]acetamide (PDBID: 3KXM), 5,6,7,8-tetrabromo-1-methyl-2,3-dihydro-1*H*-imidazo[1,2-*a*]benzimidazole (PDBID: 1ZOH) and one of two alternative orientations found for 4,5,6,7-tetrabromo-2-(methylsulfanyl)-1*H*-benzimidazole (PDBID: 1ZOG).[19,35,37]

Experimental

General procedures

Dry solvents were distilled before use and dried by standard methods. All commercially available reagents were used without further purification. Melting points (uncorrected) were determined on a Stuart Scientific SMP3 apparatus. Infrared (IR) spectra were recorded with a Perkin-Elmer 1330 infrared spectrophotometer, using KBr as solid matrix. ^{1}H and ^{13}C NMR data were recorded on a Bruker DPX 300M-BACS60 instrument. Chemical shifts (δ) are expressed in parts per million relative to solvent resonance as the internal standard; coupling constants (J) are in hertz. Mass spectra were run on a Bruker Esquire 3000 spectrometer (ESI-IT). Thin-layer chromatography (TLC) was run on Merck silica gel 60 F-254 plates and Merck silica gel 60 (230–400 mesh) was used for flash chromatography. Analytical purity of tested compound was determined either by High-performance liquid chromatography coupled to mass spectroscopy (HPLC-MS) or elemental analyses. HPLC-MS were done in Synthelia Organics SL. 1100 HPLC (Xterra MS C18 5 μm reverse phase columns) coupled to 1946D MS detector, both from Agilent, were used. Elemental analyses (C, H, N, S) were performed

on a LECO CHNS-932 apparatus at the Microanalyses Service of the Universidad Complutense de Madrid.

General method for the synthesis of 1–3. A solution of the corresponding bromoacid or carbamate (1 equiv.) and sodium azide (1.2 equiv.) in DMF was stirred overnight at 60 °C. Then the solution was extracted with AcOEt. The organic layer was washed with water and brine, dried ($MgSO_4$), filtered and evaporated to dryness. The residue was purified as specified in each case.

*tert-Butyl 2-azidoethylcarbamate (**1**).* From *tert*-butyl 2-bromoethylcarbamate (100 mg, 0.446 mmol) and sodium azide (32.7 mg, 0.535 mmol), after work-up and without further purification, **1** was obtained (69 mg, 83%) as an oil. IR (KBr) 2099, 1693, 1517 cm^{-1}; ^1H NMR (300 MHz, $CDCl_3$) δ 1.45 (s, 9H, $3CH_3$), 3.26–3.32 (m, 2H, CH_2), 3.41 (t, *J* 5.5, 2H, CH_2), 4.83 (s, H, CONH); ^{13}C NMR (75.4 MHz, $CDCl_3$) δ 28.4, 40.1, 51.2, 79.8, 155.7; MS (ESI): *m*/*z* 208.88 $[M + Na]^+$.

*tert-Butyl 3-azidopropylcarbamate (**2**).* From *tert*-butyl 3-bromopropylcarbamate (100 mg, 0.419 mmol), and sodium azide (32.7 mg, 0.503 mmol), after work-up and without further purification, **2** was obtained (76.5 mg, 91%) as an oil. IR (KBr) 2099, 1697, 1651, 1521 cm^{-1}; ^1H NMR (300 MHz, $CDCl_3$) δ 1.38 (s, 9H, $3CH_3$), 1.70 (m, 2H, CH_2), 3.14 (m, 2H, CH_2), 3.29 (t, *J* 6.7, 2H, CH_2), 4.60 (s, H, CONH); ^{13}C NMR (75.4 MHz, $CDCl_3$) δ 28.4, 29.3, 38.1, 49.1, 79.4, 155.9; MS (ESI): *m*/*z* 222.94 $[M + Na]^+$.

*tert-Butyl 4-azidobutylcarbamate (**3**).* From *tert*-butyl 4-bromobutylcarbamate (100 mg, 0.39 mmol), and sodium azide (30 mg, 0.47 mmol), after work-up and without further purification, **3** was obtained (80 mg, 94%) as an oil. IR (KBr) 2090, 1698, 1521 cm^{-1}; ^1H NMR (300 MHz, $CDCl_3$) δ 1.37 (s, 9H, $3CH_3$), 1.47–1.57 (m, 4H, $2CH_2$), 3.08 (dd, *J* 12.4, 6.2, 2H, CH_2), 3.23 (t, *J* 6.4, 2H, CH_2), 4.54 (s, H, CONH); ^{13}C NMR (75.4 MHz, $CDCl_3$) δ 26.1, 27.4, 28.3, 39.9, 51.0, 79.2, 155.9.

General method for the synthesis of 4–6. A solution of the corresponding azide (1 equiv.) and alkyne (4 equiv.) in acetone in the presence of K_2CO_3 (8 equiv.) was stirred at 60 °C and the progress of the reaction was controlled by TLC. Then the precipitate was filtered off with hot acetone and the solvent was evaporated to dryness. The residue was purified as specified in each case.

*4,5,6,7-Tetrabromo-1-(but-3-ynyl)-1H-benzo[d]triazole (**4**), and 4,5,6,7-tetrabromo-2-(but-3-ynyl)-2H-benzo[d]triazole (**5**).* From **TBB** (2.0 g, 4.6 mmol) and 4-bromobut-1-yne (2.57 g, 19.32 mmol), after work-up and purification by column chromatography on aluminum oxide, using hexane/DCM (9 : 1) as eluent, two isomers (**5** – 1.05 g, 47%, **4** – 0.14 g, 6%) were obtained. **4**: mp 191.3–192.8 °C; IR (KBr) 2119 cm^{-1}; ^1H NMR (300 MHz, DMSO) δ 2.88–2.93 (m, 3H, CH + CH_2), 5.07 (t, *J* 6.7, 2H, CH_2); ^{13}C NMR (75.4 MHz, DMSO) δ 20.5, 48.1, 74.0, 79.7, 106.9, 115.8, 123.6, 128.7, 131.8, 144.8. **5**: mp. 177.5–180.2 °C; IR (KBr) 2111 cm^{-1}; ^1H NMR (300 MHz, DMSO) δ: 3.02 (t, *J* 2.5, 1H, CH), 3.13–3.18 (m, 2H, CH_2), 5.07 (t, *J* 6.7, 2H, CH_2); ^{13}C NMR (75.4 MHz, DMSO) δ 19.1, 55.5, 73.7, 79.9, 113.6, 125.8, 142.5.

*tert-Butyl 2-(perbromo-2H-benzo[d]triazol-2-yl)ethylcarbamate (**6**).* To a solution of **TBB** (100 mg, 0.23 mmol) and K_2CO_3 (127 mg, 0.92 mmol) in acetone at RT was added *tert*-butyl 2-bromoethylcarbamate (103 mg, 0.46 mmol). The reaction mixture was stirred for 8 h at 60 °C. The precipitate was filtered off with hot acetone, and the solvent was evaporated to dryness. The residue was purify by column chromatography on aluminum oxide using hexane/AcOEt (0.5 : 9.5) to give **6** (50 mg, 38%) as a solid, mp 177.5–178.9 °C. IR (KBr) 1686, 1529 cm^{-1}; ^1H NMR (DMSO) δ 1.28 (s, 9H, $3CH_3$), 3.56 (m, 2H, CH_2), 4.81 (t, *J* 5.6, 2H, CH_2), 6.97 (br s, 1H, CONH); ^{13}C NMR (DMSO) δ 28.0, 54.8, 56.9, 77.9, 113.6, 125.2, 142.7, 155.3.

General method for the synthesis of 7, 8, 11–13. A solution of the corresponding alkyne (1 equiv.), sodium ascorbate (0.4 equiv.), $CuSO_4 \cdot 5H_2O$ (0.2 equiv.) and the corresponding azide (1 equiv.) in DMF was stirred for 48 h at RT. Then, the solution was extracted with DCM. The organic layer was washed with water and brine, dried ($MgSO_4$), filtered and evaporated to dryness. The residue was purified as specified in each case.

*tert-Butyl 3-(3-(2-(perbromo-1H-benzo[d]triazol-1-yl)ethyl)-1H-pyrrol-1-yl)propylcarbamate (**7**).* From **4** (200 mg, 0.41 mmol), and **2** (91 mg 0.45 mmol), after work-up and purification by column chromatography using DCM/MeOH (9.9 : 0.1) as eluent, **7** (220 mg, 78%) was obtained as a solid, mp 102.6–104.3 °C. IR (KBr) 1695, 1516 cm^{-1}; ^1H NMR (300 MHz, DMSO) δ 1.38 (s, 9H, $3CH_3$), 1.86 (m, *J* 6.8, 2H, CH_2), 2.90 (dd, *J* 12.5, 6.4, 2H, CH_2), 3.46–3.22 (m, 2H, CH_2), 4.28 (t, *J* 7.0, 2H, CH_2), 5.18 (t, *J* 7.2, 2H, CH_2), 6.92 (t, *J* 5.3, 1H, CONH), 7.90 (s, 1H, CH-triazole); ^{13}C NMR (75.4 MHz, DMSO) δ 26.9, 28.1, 30.2, 36.9, 46.9, 49.4, 77.6, 106.6, 115.7, 123.0, 123.4, 128.4, 131.7, 142.0, 144.8, 155.5.

*tert-Butyl 2-(3-(2-(perbromo-1H-benzo[d]triazol-1-yl)ethyl)-1H-pyrrol-1-yl)ethylcarbamate (**8**).* From **4** (200 mg, 0.41 mmol) and **1** (84 mg 0.45 mmol), after work-up and purification by column chromatography using DCM/MeOH (9.9 : 0.1) as eluent, **8** (220 mg, 79%) was obtained as a solid, mp 121.4–122.8 °C. IR (KBr) 1711, 1516 cm^{-1}; ^1H NMR (300 MHz, DMSO) δ 1.35 (s, 9H, $3CH_3$), 2.49–2.52 (m, 4H, $2CH_2$), 4.33 (t, *J* 6.2, 2H, CH_2), 5.17 (t, *J* 7.3, 2H, CH_2), 6.97 (t, *J* 5.6, 1H, CONH), 7.90 (s, 1H, CH-triazole); ^{13}C NMR (75.4 MHz, DMSO) δ 26.9, 28.1, 48.9, 49.4, 77.9, 106.6, 115.7, 123.1, 123.4, 128.4, 131.7, 142.0, 144.8, 155.4.

*tert-Butyl 4-(4-(2-(perbromo-2H-benzo[d]triazol-2-yl)ethyl)-1H-1,2,3-triazol-1-yl) butylcarbamate (**11**).* From **5** (180 mg, 0.373 mmol) and **3** (80 mg, 0.373 mmol), after work-up and purification by column chromatography using DCM/MeOH (9.75 : 0.25) as eluent, **11** (258 mg, 99%) was obtained as a solid. IR (KBr) 1682, 1521 cm^{-1}; ^1H NMR (300 MHz, $CDCl_3$) δ 1.43 (s, 9H, $3CH_3$), 1.40–1.56 (m, 2H, CH_2), 1.87–1.94 (m, 2H, CH_2), 3.14 (dd, *J* 13.1, 6.6, 2H, CH_2), 3.59 (t, *J* 7.2, 2H, CH_2), 4.33 (t, *J* 7.1, 2H, CH_2), 4.61 (s, H, CONH), 5.10 (t, *J* 7.2, 2H, CH_2), 7.28 (s. 1H, CH-triazole); ^{13}C NMR (75.4 MHz, $CDCl_3$) δ 26.3, 27.1, 27.4, 28.3, 39.6, 49.7, 56.6, 79.3, 113.7, 121.7, 126.4, 142.8, 143.1, 156.0; MS (ESI): *m*/*z* 175.92 $[M + H–Br]^+$.

*tert-Butyl 3-(4-(2-perbromo-2H-benzo[d]triazol-2-yl)-1H-1,2,3-triazol-1-yl)propylcarbamate (**12**).* From **5** (170 mg, 0.349 mmol) and **2** (69 mg, 0.349 mmol), after work-up and purification by column chromatography using DCM/MeOH (9.5 : 0.5) as eluent, **12** (220 mg, 92%) was obtained as a solid, mp 175.5–177.6 °C. IR (KBr) 1682, 1525 cm^{-1}; ^1H NMR (300 MHz, $CDCl_3$) δ 1.37 (s, 9H, $3CH_3$), 1.96 (m, 2H, CH_2), 3.02 (q, 2H, CH_2), 3.53 (t, *J* 7.2, 2H, CH_2), 4.28 (t, *J* 6.7, 2H, CH_2), 4.65 (s, 1H, CONH), 5.02 (t, *J* 7.2, 2H, CH_2), 7.19 (s. 1H, CH-triazole); ^{13}C NMR (75.4 MHz, $CDCl_3$)

δ 26.3, 28.3, 30.8, 37.2, 47.4, 56.6, 79.6, 113.8, 122.2, 126.5, 142.8, 143.1, 156.0.

*tert-Butyl 2-(4-(2-(perbromo-1H-benzo[d]triazol-2-yl)ethyl)-1H-1,2,3-triazol-1-yl)ethylcarbamate (**13**).* From **5** (200 mg, 0.41 mmol) and **1** (70 mg 0.41 mmol), after work-up and purification by column chromatography using DCM/MeOH (9.75 : 0.25) as eluent, **13** (160 mg, 60%) was obtained as a solid, mp 193.3–195.9 °C. IR (KBr) 1674, 1521 cm^{-1}; ^1H NMR (300 MHz, $CDCl_3$) δ 1.35 (s, 9H, $3CH_3$), 3.50–3.55 (m, 4H, $2CH_2$), 4.34 (t, *J* 5.7, 2H, CH_2), 4.78 (br s, H, CONH) 5.02 (t, *J* 7.3, 2H, CH_2), 7.19 (s, 1H, CH-triazole); ^{13}C NMR (75.4 MHz, $CDCl_3$) δ 26.2, 28.3, 40.5, 50.0, 56.5, 80.1, 113.8, 122.5, 126.5, 143.0, 143.2.

General method for the synthesis of 9, 10, 14–16, 17. A solution of the corresponding carbamate (1 equiv.) and TFA (10 equiv.) in DCM was stirred at RT, and the progress of the reaction was controlled by TLC. The crude was neutralized with 0.1 M NaOH at 0 °C. Then, DCM was added and the organic solution was washed with water, dried ($MgSO_4$), filtered and evaporated to dryness. The residue was purified as specified in each case.

*3-(4-(2-(Perbromo-1H-benzo[d]triazol-1-yl)ethyl)-1H-1,2,3-triazol-1-yl)propan-1-amine (**9**).* From **7** (150 mg, 0.21 mmol), after work-up and purification by column chromatography using DCM/MeOH (9.5 : 0.5) as eluent, **9** (100 mg, 69%) was obtained as a solid, mp 152.4–154.7 °C. IR (KBr) 3432 cm^{-1}; ^1H NMR (300 MHz, DMSO) δ 1.80 (m, 2H, CH_2), 2.49–2.51 (m, 2H, CH_2), 3.33 (t, *J* 7.1, 2H, CH_2), 4.33 (t, *J* 7.0, 2H, CH_2), 5.18 (t, *J* 7.1, 2H, CH_2), 7.86 (s, 1H, CH-triazole); ^{13}C NMR (75.4 MHz, DMSO) δ 26.9, 33.3, 38.1, 46.9, 49.4, 106.7, 115.7, 122.9, 123.4, 131.7, 141.9, 144.8; Anal Calcd for $C_{13}H_{13}Br_4N_7$: C, 26.60; H, 2.23; N, 16.71. Found: C, 26.55; H, 2.53; N, 16.02.

*2-(4-(2-(Perbromo-1H-benzo[d]triazol-1-yl)ethyl)-1H-1,2,3-triazol-1-yl)ethanamine (**10**).* From **8** (140 mg, 0.2 mmol) after work-up and purification by column chromatography using DCM/MeOH (9.5 : 0.5) as eluent, **10** (80 mg, 63%) was obtained as a solid, mp 183.7–185.6 °C. IR (KBr) 3373 cm^{-1}; ^1H NMR (300 MHz, DMSO) δ 2.90 (t, *J* 6.1, 2H, CH_2), 3.33 (t, *J* 7.2, 2H, CH_2), 4.25 (t, *J* 6.2, 2H, CH_2), 5.18 (t, *J* 7.2, 2H, CH_2), 7.88 (s, 1H, CH-triazole); ^{13}C NMR (75.4 MHz, DMSO) δ 27.0, 41.8, 49.4, 52.5, 106.7, 115.7, 123.1, 123.4, 128.4, 131.7, 141.8, 144.8; MS (ESI): *m*/*z* 573.60 $[M + H]^+$; Anal. $C_{12}H_{11}Br_4N_7$ (C, H, N, O).

*4-(4-(2-(Perbromo-2H-benzo[d]triazol-2-yl)ethyl)-1H-1,2,3-triazol-1-yl)butan-1-amine (**14**).* From **11** (120 mg, 0.17 mmol) after work-up and purification by column chromatography using DCM/MeOH (9.5 : 0.5), **14** (100 mg, 97%) was obtained as a solid, mp 166.9–168.1 °C. IR (KBr) 3126 cm^{-1}; ^1H NMR (300 MHz, DMSO) δ 1.17–1.27 (m, 2H, CH_2), 1.70–1.79 (m, 2H, CH_2), 3.45 (t, *J* 7.0, 2H, CH_2), 4.26 (t, *J* 7.0, 2H, CH_2), 5.07 (t, *J* 7.0, 2H, CH_2), 7.80 (s, H, CH-triazole); ^{13}C NMR (75.4 MHz, DMSO) δ 25.7, 27.2, 29.5, 40.7, 49.2, 56.5, 113.6, 122.7, 125.5, 142.2, 142.5; MS (ESI): *m*/*z* 601.63 $[M + H]^+$; anal. $C_{14}H_{15}Br_4N_7$ (C, H, N, O).

*3-(4-(2-(Perbromo-2H-benzo[d]triazol-2-yl) ethyl)-1H-1,2,3-triazol-1-yl)propan-1-amine (**15**).* From **12** (97 mg, 0.14 mmol), after work-up and purification by column chromatography using DCM/MeOH (9.5 : 0.5), **15** (70 mg, 82%) was obtained as a solid, mp 163.9–165.5 °C. IR (KBr) 3381 cm^{-1}; ^1H NMR (300 MHz, $CDCl_3$) δ 1.90 (m, 2H, CH_2), 2.60 (t, *J* 6.6, 2H, CH_2), 3.52 (t, *J* 7.2, 2H, CH_2), 4.34 (t, *J* 6.6, 2H, CH_2), 5.02 (t, *J* 7.2, 2H, CH_2), 7.20 (s, 1H, CH-triazole); ^{13}C NMR (75.4 MHz, $CDCl_3$) δ 25.3, 32.4, 37.6, 46.6, 55.7, 112.8, 120.8, 125.5, 141.8, 142.2; MS (ESI): *m*/*z* 587.62 $[M + H]^+$; Anal. Calcd for $C_{13}H_{13}Br_4N_7$: C, 26.60; H, 2.23; N 16.71. Found: C, 26.70; H, 2.30; N, 16.02.

*2-(4-(2-(Perbromo-2H-benzo[d]triazol-2-yl)ethyl)-1H-1,2,3-triazol-1-yl)ethanamine (**16**).* From **13** (90 mg, 0.13 mmol), after work-up and purification by column chromatography using DCM/MeOH (9.5 : 0.5), **16** (60 mg, 71%) was obtained as a solid, mp 140.7–142.7 °C. IR (KBr) 3370 cm^{-1}; ^1H NMR (300 MHz, $CDCl_3$) δ 3.09 (t, *J* 7.2, 2H, CH_2), 3.53 (t, *J* 7.2, 2H, CH_2), 4.26 (t, *J* 7.2, 2H, CH_2), 5.03 (t, *J* 7.2, 2H, CH_2), 7.19 (s. 1H, CH-triazole); ^{13}C NMR (75.4 MHz, $CDCl_3$) δ 26.3, 41.9, 53.4, 56.6, 113.8, 122.4, 126.5, 142.8, 143.2; MS (ESI): *m*/*z* 573.62 $[M + H]^+$; Anal. $C_{12}H_{11}Br_4N_7$ (C, H, N, O).

*2-(Perbromo-2H-benzo[d] triazol-2-yl)ethanamine (**17**).* From **6** (640 mg, 1.1 mmol), after work-up and purification by column chromatography using DCM/MeOH (9.5 : 0.5), **17** (480 mg, 90%) was obtained as a solid, mp 159.8–161.5 °C. IR (KBr) 3356 cm^{-1}; ^1H NMR (300 MHz, DMSO) δ 1.83 (br s, 2H, NH_2), 3.21 (t, *J* 6.0, 2H, CH_2), 4.76 (t, *J* 6.0, 2H, CH_2). ^{13}C NMR (75.4 MHz, DMSO) δ 41.7, 60.3, 113.5, 125.2, 142.5; Anal. $C_8H_6Br_4N_4$ (C, H, N, O).

*tert-Butyl 2-oxo-2-(2-(perbromo-2H-benzo[d]triazol-2-yl)ethylamino) ethyl carbamate (**18**).* A solution of 2-(*tert*-butoxycarbonylamino) acetic acid (86.1 mg, 0.492 mmol), HOBT (83.1 mg 0.615 mmol), NMM (124.41 mg 1.23 mmol) and **17** (200 mg, 0.41 mmol) was stirred overnight in DMF at RT. Then, the solution was extracted with AcOEt. The organic layer was washed with ammonium chloride and brine, dried ($MgSO_4$), filtered and evaporated to dryness. The residue was purify by column chromatography using DCM/MeOH 9.9 : 0.1 as eluent to give **18** (250 mg, 94%) as a solid, mp 189.7–191.6 °C. IR (KBr) 1712, 1671, 1511 cm^{-1}; ^1H NMR (300 MHz, DMSO) δ 1.34 (s, 9H, $3CH_3$), 3.44 (d, *J* 6.0, 2H, CH_2), 3.74 (d, *J* 5.7, 2H, CH_2), 4.83 (t, *J* 5.8, 2H, CH_2), 6.89 (t, *J* 5.9, 1H, CONH), 7.97 (t, *J* 5.6, 1H, CONH); ^{13}C NMR (75.4 MHz, DMSO) δ 28.0, 38.4, 43.0, 56.2, 77.9, 113.6, 125.4, 142.6, 155.5, 169.8.

*2-Amino-N-(2-(perbromo-2H-benzo[d]triazol-2-yl)ethyl)acetamide (**19**).* From **18** (205 mg, 0.15 mmol), after work-up and purification by column chromatography using DCM/MeOH (9.9 : 0.1), **19** (90 mg, 79%) was obtained as a solid, mp 187.7–189.4 °C. IR (KBr) 1646, 1526 cm^{-1}. ^1H NMR (300 MHz, DMSO) δ 1.94 (br s, 2H, NH_2), 3.03 (s, 2H, CH_2), 3,74 (d, *J* 5.4, 2H, CH_2), 4.85 (t, *J* 5.8, 2H, CH_2), 8.08 (br s, 1H, CONH); ^{13}C NMR (75.4 MHz, DMSO) δ 38.3, 44.6, 56.4, 113.6, 125.4, 142.6, 173.4; MS (ESI): *m*/*z* 569.61 $[M + H–Br]^+$; anal. $C_{10}H_9Br_4N_5O$ (C, H, N, O).

*4-Hydroxy-N-(2-(perbromo-2H-benzo[d]triazol-2-yl)ethyl)butanamide (**20**).* A solution of **17** (100 mg, 0.21 mmol) and γ-butyrolactone (18 mg, 0.21 mmol) in toluene was stirred for 24 h under reflux. DCM was added to the crude, and the organic solution was washed with water, dried ($MgSO_4$), filtered and evaporated to dryness. The residue was recrystallized from EtOH/AcOEt to give **20** (50 mg, 42%) as a solid, mp 122.3–125.5 °C. IR (KBr) 3272, 1651, 1570 cm^{-1}; ^1H NMR (300 MHz, DMSO) δ 1.52–1.62 (m, 2H, CH_2), 2.03 (t, *J* 7.2, 2H, CH_2), 3.33 (dd, *J* 11.5, 6.4, 2H, CH_2), 3.67 (dd, *J* 11.5, 5.8, 2H, CH_2), 4.40 (t, *J* 5.2, 1H, OH), 4.83 (t, *J* 5.7, 2H, CH_2), 7.93 (t, *J* 5.8, 1H, CONH); ^{13}C NMR (75.4 MHz, DMSO) δ 28.5, 32.0, 56.4, 60.1, 113.6,

125.3, 142.6, 172.6; MS (ESI): *m/z* 560.66 $[M + H]^+$; anal. $C_{12}H_{12}Br_4N_4O_2$ (C, H, N, O).

*4-Oxo-4-(2-(perbromo-2H-benzo[d]triazol-2-yl)ethylamino)butanoic acid (**21**).* A solution of **17** (100 mg, 0.093 mmol) and succinic anhydride (13.95 mg, 0.139 mmol) in EtOH was stirred for 24 h at 45 °C. Then, AcOEt was added to the reaction mixture and the organic layer was washed with water and brine, dried ($MgSO_4$), filtered and evaporated to dryness. The residue was purify by recrystallization from EtOH to give **21** (80 mg, 66%) as a solid, mp 231.3–232.4 °C. IR (KBr) 1715, 1635, 1554 cm^{-1}; ^1H NMR (300 MHz, DMSO) δ 2.25 (t, *J* 6.8, 2H, CH_2), 2.38 (dd, *J* 10.8, 3.8, 2H, CH_2), 3.69 (dd, *J* 11.6, 5.8, 2H, CH_2), 4.82 (t, *J* 5.8, 2H, CH_2), 8.01 (t, *J* 5.8, 1H, CONH), 12.07 (br s, 1H, COOH); ^{13}C NMR (75.4 MHz, DMSO) δ 29.0, 29.9, 56.3, 113.6, 125.4, 142.6, 171.4, 173.5; MS (ESI): *m/z* 578.60 $[M + H]^+$; Anal $C_{12}H_{10}Br_4N_4O_3$ (C, H, N, O).

*5-Oxo-5-(2-(perbromo-2H-benzo[d]triazol-2-yl)ethylamino)pentanoic acid (**22**).* A solution of **17** (100 mg, 0.093 mmol) and glutaric anhydride (15.9 mg, 0.14 mmol) in EtOH was stirred for 24 h at 45 °C. Then, AcOEt was added to the reaction mixture and the organic layer was washed with water and brine, dried ($MgSO_4$), filtered and evaporated to dryness. The residue was purify by column chromatography using DCM/MeOH (9.75 : 0.25) to give **22** (75 mg, 61%) as a solid, mp 200.2–201.4 °C. IR (KBr) 1721, 1613, 1548 cm^{-1}; ^1H NMR (300 MHz, DMSO) δ 1.65 (m, 2H, CH_2), 2.03 (t, *J* 7.4, 2H, CH_2), 2.15 (t, *J* 7.4, 2H, CH_2), 3.67 (dd, *J* 11.4, 5.7, 2H, CH_2), 4.83 (t, *J* 5.7, 2H, CH_2), 7.94 (t, *J* 5.8, 1H, CONH), 11.95 (s, 1H, COOH); ^{13}C NMR (75.4 MHz, DMSO) δ 20.5, 32.9, 34.3, 56.4, 113.5, 125.3, 142.6, 172.1, 174.0; MS (ESI): *m/z* 592.60 $[M + H]^+$; anal. $C_{13}H_{12}Br_4N_4O_3$ (C, H, N, O).

Human CK2 catalytic subunits α and α' were expressed and purified according to the method described by Frączyk *et al.*[38] Human CK2 α and α' were expressed as fusion proteins with N-terminal GST, a set of the corresponding plasmids, pGEX-3x:CK2α, pGEX-3x:CK2α' and pGEX3x:CK2β, a generous gift from Prof. D. Litchfield, University of Western Ontario. The plasmids were used to transform *E. coli* BL21 trxB DE3 cells (applied for further protein overexpression) which were cultured in LB medium containing ampicillin and kanamycin at final concentrations of 100 and 10 μg mL^{-1}, respectively. Overexpression was induced by IPTG addition to a final concentration of 0.1 mM just after the OD600 attained a value of 0.5. After 24 h incubation at 30 °C, cells were harvested, rinsed with TBS and stored at −70 °C. Following overexpression of GST-CK2α/α', bacterial cells were resuspended in lysis buffer containing 50 mM Tris–HCl, pH 7.5, 300 mM NaCl, 0.5 mM PMSF and 6 mM β-ME, and sonicated. The resulting suspension was centrifuged 15 min at 15 000 rpm, and a sample of the supernatant loaded on a 1 ml column of glutathione–agarose beads. Unbound protein was washed out with TBS buffer containing 1% Triton X-100, and the appropriate GST-CK2 subunit was eluted (elution buffer containing 50 mM Tris–HCl, pH 9.4, and 10 mM reduced glutathione). Eluted proteins were collected as 0.5 ml fractions and analyzed on 11.25% SDS/PAGE. Fractions containing pure GST-CK2 subunit were combined (purity over 85%), dialyzed against TBS buffer containing 20% glycerol, concentrated and stored at −20 °C. Protein concentration was determined with Broadford method. Activity of CK2 catalytic subunits was determined as the rate of incorporation of phosphate from [γ-32P]ATP into the RRRDDDSDDD peptide substrate under conditions described below.

Determination of CK2 activity

The mixture reaction (50 μl) containing 4 pmol CK2α or CK2α' (spec. act. 2 μmol min^{-1} mg), peptide substrate (40 μM, RRRADDSDDDDD, SIGMA); Tris–HCl pH 7.5 (20 mM); 6 mM 2-mercaptoethanol and $MgCl_2$ (10 mM), 0–100 μM [γ-^{32}P]ATP (Hartman Analytics GmbH) was incubated for 10 min at 37 °C. 10 μL of the assay mixture was spotted onto a square (1 cm × 1 cm) of Whatman P81 paper, and allowed to dry. Each square was immersed in cold 0.5% phosphoric acid, and washed 3 times during 10 min. Then the squares were washed with 96% EtOH, allowed to dry and transferred into a vessel containing Opti Phase liquid (scintillation solution) and radioactivity was quantified using a BECKMAN LS6500. The activity was calculated as the percentage of incorporated ^{32}P-phosphate (measured in scintillation counter).

Inhibition studies were performed at fixed concentrations of substrate and at variable concentrations of ATP in the absence or in the presence of increasing concentrations of inhibitor. Kinetic parameters were determined by non-linear-regression analysis using competition binding equation as "One site fit K_i", GraphPad Prism 4.0 (GraphPad Software, Inc San Diego).

All experiments were performed in triplicate.

Cell lines experiments

Human T-leukemia cells of Jurkat line were obtained from cell culture collection of Institute of Cancer Research, Vienna Medical University (Vienna, Austria) and murine leukemia cells of L1210 line were obtained from cell culture collection of R. E. Kavetsky Institute of Experimental Pathology, Oncology and Radiobiology, National Academy of Sciences of Ukraine (Kyiv, Ukraine). Human breast adenocarcinoma cells of MCF-7 and MDA-MD-231 lines were obtained from Ludwig Institute for Cancer Research (Uppsala, Sweden). Jurkat cells were cultured in the RPMI medium, while all other cells were cultured in DMEM medium, supplemented with 10% fetal calf serum (Sigma Chemical Co., St. Louis, USA), 50 μg mL^{-1} streptomycin (Sigma Chemical Co., St. Louis, USA), 50 units per mL penicillin (Sigma Chemical Co., St. Louis, USA) in 5% CO_2-containing humidified atmosphere at 37 °C.

For experiments, cells were seeded into 24-well tissue culture plates (Greiner Bio-one, Germany). 2 mM stock solutions of each CK2 inhibitor in DMSO (99.5% pure, Sigma, USA) were prepared, and additionally dissolved in serum-free culture medium (RPMI for leukemia cells and DMEM for carcinoma cells) prior to addition to cell culture. Final concentration of DMSO in cell culture was 0.5% or less. Cytotoxicity studies on Jurkat and MCF-7 cells revealed no statistically significant toxicity of 0.5% DMSO solution on these cell lines.

Cytotoxic effect of antitumor drugs was studied under the light microscope (Evolution 300, Delta Optical, Poland) after cell staining with trypan blue dye (0.1%).

FITC-conjugated Annexin V (BD Pharmingen, USA) and propidium iodide (Sigma, USA) double staining were performed to detect early apoptotic events under treatment of Jurkat cells by CK2 inhibitors. In 24 h after the addition of **35**, **14**, **16** Jurkat cells were centrifuged at 2.000 rpm, washed twice with 1× PBS, and incubated for 15 min in Annexin V binding buffer (BD Pharmingen, USA) containing 1/20 volume of FITC-conjugated Annexin V solution and PI (20 μg mL^{-1}). 10 μL of cell suspension were added to slides and cover glasses placed. Cytomorphological investigations were performed on Zeiss AxioImager A1 fluorescent microscope.

DAPI staining was performed for studying chromatin condensation in MCF-7 cells under **10**, **14**, **16** treatment. 24 h after the addition of CK2 inhibitors, MCF-7 cells were washed twice with 1× PBS, fixed in 4% solution of paraformaldehyde for 15 min at room temperature, and then permeabilized by 0.1% Triton X-100 solution in PBS for 3 min. After that, cells were incubated with 1 μg mL^{-1} solution of DAPI (4′,6-diamidino-2-phenylindole) (Sigma, USA) for 5 min, washed twice with PBS and cover glasses with fixed cells were placed on slides. Cytomorphological investigations were performed on Zeiss AxioImager A1 fluorescent microscope (Zeiss, Germany).

All experiments were performed in triplicate.

Computational studies

Preparation of the protein structure. We selected the X-ray structure of CK2 in complex with ANP (3NSZ.pdb) as a target protein for the initial docking studies. The final docking studies were carried out with the near-end versions of 5CQU and 5CQW. All Mg^{2+} ions were removed in the 3NSZ experimental structure and all sulphates, co-solvents and water molecules were removed from the near-end versions of 5CQU and 5CQW. The proteins were prepared with the protein preparation wizard[39] provided in Schrödinger suite and a minimization was performed until the RMSD value of all heavy atoms was within 0.3 Å of the crystal structure. Grids were constructed with the grid receptor generation module included in Glide software. The binding pocket was identified by placing a 20 Å cube around the geometrical center of AMP-PNP. The ligands (**9–17**, **19–22**) were prepared using LigPrep[40] application also provided in the Schrödinger suite. Amino groups were considered as protonated. The 2005 implementation of the OPLS-AA force field and a van der Waals radii scale factor of 1.0/0.8 were used for receptor and ligands, respectively. During the docking calculations, all the protein residues were fixed and only the inhibitor atoms were allowed to move. Flexible docking calculations were carried out with the Glide program,[41,42] using default parameters and requiring a maximum of ten output poses. We selected the XP (Extra-Precision) method allowing a more extensive sampling method, as well as a more exigent scoring function.[43,44] Binding poses presented favorable theoretical binding energies within the range of −10 to −3 kcal mol^{-1}.

Crystallography

For crystallographic studies a C-terminally truncated, but fully active construct of human CK2α (*hs*CK2α^{1-335}) was used.[44] *Hs*CK2α^{1-335} was expressed recombinantly in *Escherichia coli* BL21(DE3) cells and purified according to the original protocol[44] and a later modification.[45] The final protein stock solution had the following composition: 12 mg mL^{-1} *hs*CK2α^{1-335}, 500 mM NaCl, 25 mM Tris/HCl, pH 8.5. For all subsequent crystallization experiments the sitting-drop variant of the vapor diffusion method was applied. Complexes of *hs*CK2α^{1-335} and the inhibitor were generated by:

(a) pre-incubation/co-crystallization: the following *hs*CK2α^{1-335}/inhibitor solution was prepared and incubated for 30 min at room temperature prior to crystallization: 6 mg mL^{-1} *hs*CK2α^{1-335}, 1 mM inhibitor, 10% (v/v) DMSO, 250 mM NaCl, 12.5 mM Tris/HCl, pH 8.5. For co-crystallization 1 μL of this solution was mixed with 1 μL reservoir solution composed of 25% (w/v) PEG3350, 0.2 M Li_2SO_4, 0.1 M Bis-Tris/HCl, pH 5.5. The mixture was equilibrated at 20 °C against this reservoir solution. For X-ray diffractometry single crystals were dipped into a cryo solution composed of 25% (w/v) PEG3350, 15% (v/v) glycerol, 0.2 M Li_2SO_4, 0.1 M Bis-Tris/HCl, pH 5.5.

(b) Ligand exchange by soaking: the following *hs*CK2α^{1-335}/AMP-PNP solution was prepared prior to crystallization: 6 mg mL^{-1} *hs*CK2α^{1-335}, 440 μM AMP-PNP, 890 μM $MgCl_2$, 250 mM NaCl, 12.5 mM Tris/HCl, pH 8.5. 1 μL of this solution was mixed with 1 μL reservoir solution composed of 30% (w/v) PEG4000, 0.2 M Li_2SO_4, 0.1 M Tris/HCl, pH 8.5. The mixture was equilibrated at 20 °C against this reservoir solution. *Hs*CK2α^{1-335}/AMP-PNP crystals forming under these conditions were then soaked for one week in reservoir solution complemented with 3 mg mL^{-1} *hs*CK2α^{1-335}, 300 μM inhibitor and 890 μL $MgCl_2$. For X-ray diffractometry single crystals were dipped into a cryo solution composed of 30% (w/v) PEG4000, 15% (v/v) glycerol, 0.2 M Li_2SO_4, 0.1 M Tris/HCl, pH 8.5. X-ray diffraction data sets were collected at 100 K at the X06Da-PXIII beamline at the Swiss Light Source (SLS) in Villingen, Switzerland, and European Synchrotron Radiation Facility (ESRF) in Grenoble, France. The data were integrated with XDS[46] and scaled with SCALA[47] from the CCP4 software suite.[48] The crystallographic refinement including parametrization of the inhibitor was performed with PHENIX[49] and started with two isomorphous structures from the Protein Data Bank, namely 2PVR (soaked crystal) and 3NGA[50] (crystal from co-crystallization). For manual corrections we used COOT.[51] In the final structures the bromine atoms are unambiguously visible, but their atomic B-factors are distinctly higher than those of the benzotriazole core atoms; this observation is probably due to a certain degree of radiation damage because bromine shows significant X-ray absorption at 1 Å, the wavelength used for diffractometry (Table 4). The final atomic coordinates and the experimental structure factor amplitudes are available from the PDB under the accession codes 5CQU (monoclinic *hs*CK2α^{1-335}/inhibitor structure from soaking) and 5CQW (tetragonal *hs*CK2α^{1-335}/inhibitor structure from co-crystallization).

Conclusions

In conclusion, we have demonstrated that the introduction of an aminoalkyl chain in TBB improves the permeability

properties of the molecule. Thus, although there is a loss of inhibitory activity against CK2 *in vitro*, the cytotoxic activity developed by our best compounds in leukemia and breast cancer cells is similar or higher than the activity described for TBB in the same tumor cells. It is well known that a higher expression and activity of CK2 creates a more favorable environment for tumor development. Development of new strategies to inhibit CK2 abnormal activity is important to understand the behavior of this enzyme. On the other hand, the new set of inhibitors described here and the study of their mode of binding can provide the basis for future structure based design of improved ATP-competitive CK2 inhibitors.

Acknowledgements

This work was supported by the Spanish Ministry of Science and Innovation (CTQ2011-24741), and by the Deutsche Forschungsgemeinschaft (DFG; grant NI 643/4-1). We thank Airbus Military for fellowships to RS and MM. We thank also Synthelia Organics SL. for HPLC-MS experiments and the staff at the SLS in Villingen and the ESRF in Grenoble for assistance with synchrotron diffraction experiments.

Notes and references

1 D. W. Litchfield, *Biochem. J.*, 2003, **369**, 1–15.
2 B. Guerra and O. G. Issinger, *Curr. Med. Chem.*, 2008, **15**, 1870–1886.
3 J. S. Duncan and D. W. Litchfield, *Biochim. Biophys. Acta*, 2008, **1784**, 33–47.
4 T. Buchou, M. Vernet, O. Blond, H. H. Jensen, H. Pointu, B. B. Olsen, C. Cochet, O. G. Issinger and B. Boldyreff, *Mol. Cell. Biol.*, 2003, **23**, 908–915.
5 D. Escalier, D. Silvius and X. Xu, *Mol. Reprod. Dev.*, 2003, **66**, 190–201.
6 C. V. Glover 3rd, *Prog. Nucleic Acid Res. Mol. Biol.*, 1998, **59**, 95–133.
7 D. Y. Lou, I. Dominguez, P. Toselli, E. Landesman-Bollag, C. O'Brien and D. C. Seldin, *Mol. Cell. Biol.*, 2008, **28**, 131–139.
8 A. Hessenauer, C. C. Schneider, C. Goetz and M. Montenarh, *Cell. Signalling*, 2011, **23**, 145–151.
9 G. Cozza, L. A. Pinna and S. Moro, *Curr. Med. Chem.*, 2013, **20**, 671–693.
10 X. Cheng, K.-H. Merz, S. Vatter, J. Christ, S. Woelfl and G. Eisenbrand, *Bioorg. Med. Chem.*, 2014, **22**, 247–255.
11 A. G. Golub, V. G. Bdzhola, O. V. Ostrynska, I. V. Kyshenia, V. M. Sapelkin, A. O. Prykhod'ko, O. P. Kukharenko and S. M. Yarmoluk, *Bioorg. Med. Chem.*, 2013, **21**, 6681–6689.
12 G. Cozza, C. Girardi, A. Ranchio, G. Lolli, S. Sarno, A. Orzeszko, Z. Kazimierczuk, R. Battistutta, M. Ruzzene and L. A. Pinna, *Cell. Mol. Life Sci.*, 2014, **71**, 3173–3185.
13 H. Sun, X. Xu, X. Wu, X. Zhang, F. Liu, J. Jia, X. Guo, J. Huang, Z. Jiang, T. Feng, H. Chu, Y. Zhou, S. Zhang, Z. Liu and Q. You, *J. Chem. Inf. Model.*, 2013, **53**, 2093–2102.
14 B. Kaminska, A. Ellert-Miklaszewska, A. Oberbek, P. Wisniewski, B. Kaza, M. Makowska, M. Bretner and Z. Kazimierczuk, *Int. J. Oncol.*, 2009, **35**, 1091–1100.
15 M. Makowska, E. Lukowska-Chojnacka, P. Winska, A. Kus, A. Bilinska-Chomik and M. Bretner, *Mol. Cell. Biochem.*, 2011, **356**, 91–96.
16 A. Najda-Bernatowicz, M. Lebska, A. Orzeszko, K. Kopanska, E. Krzywinska, G. Muszynska and M. Bretner, *Bioorg. Med. Chem.*, 2009, **17**, 1573–1578.
17 S. Sarno, S. Moro, F. Meggio, G. Zagotto, D. Dal Ben, P. Ghisellini, R. Battistutta, G. Zanotti and L. A. Pinna, *Pharmacol. Ther.*, 2002, **93**, 159–168.
18 M. A. Pagano, M. Andrzejewska, M. Ruzzene, S. Sarno, L. Cesaro, J. Bain, M. Elliott, F. Meggio, Z. Kazimierczuk and L. A. Pinna, *J. Med. Chem.*, 2004, **47**, 6239–6247.
19 R. Battistutta, M. Mazzorana, S. Sarno, Z. Kazimierczuk, G. Zanotti and L. A. Pinna, *Chem. Biol.*, 2005, **12**, 1211–1219.
20 G. Cozza, P. Bonvini, E. Zorzi, G. Poletto, M. A. Pagano, S. Sarno, A. Donella-Deana, G. Zagotto, A. Rosolen, L. A. Pinna, F. Meggio and S. Moro, *J. Med. Chem.*, 2006, **49**, 2363–2366.
21 F. Pierre, P. C. Chua, S. E. O'Brien, A. Siddiqui-Jain, P. Bourbon, M. Haddach, J. Michaux, J. Nagasawa, M. K. Schwaebe, E. Stefan, A. Vialettes, J. P. Whitten, T. K. Chen, L. Darjania, R. Stansfield, K. Anderes, J. Bliesath, D. Drygin, C. Ho, M. Omori, C. Proffitt, N. Streiner, K. Trent, W. G. Rice and D. M. Ryckman, *J. Med. Chem.*, 2011, **54**, 635–654.
22 R. Battistutta, G. Cozza, F. Pierre, E. Papinutto, G. Lolli, S. Sarno, S. E. O'Brien, A. Siddiqui-Jain, M. Haddach, K. Anderes, D. M. Ryckman, F. Meggio and L. A. Pinna, *Biochemistry*, 2011, **50**, 8478–8488.
23 A. Siddiqui-Jain, D. Drygin, N. Streiner, P. Chua, F. Pierre, S. E. O'Brien, J. Bliesath, M. Omori, N. Huser, C. Ho, C. Proffitt, M. K. Schwaebe, D. M. Ryckman, W. G. Rice and K. Anderes, *Cancer Res.*, 2010, **70**, 10288–10298.
24 R. Swider, M. Maslyk, S. Martin-Santamaria, A. Ramos and B. de Pascual-Teresa, *Mol. Cell. Biochem.*, 2011, **356**, 117–119.
25 R. Szyszka, N. Grankowski, K. Felczak and D. Shugar, *Biochem. Biophys. Res. Commun.*, 1995, **208**, 418–424.
26 M. A. Fabian, W. H. Biggs, D. K. Treiber, C. E. Atteridge, M. D. Azimioara, M. G. Benedetti, T. A. Carter, P. Ciceri, P. T. Edeen, M. Floyd, J. M. Ford, M. Galvin, J. L. Gerlach, R. M. Grotzfeld, S. Herrgard, D. E. Insko, M. A. Insko, A. G. Lai, J. M. Lelias, S. A. Mehta, Z. V. Milanov, A. M. Velasco, L. M. Wodicka, H. K. Patel, P. P. Zarrinkar and D. J. Lockhart, *Nat. Biotechnol.*, 2005, **23**, 329–336.
27 C. Carvalho, R. X. Santos, S. Cardoso, S. Correia, P. J. Oliveira, M. S. Santos and P. I. Moreira, *Curr. Med. Chem.*, 2009, **16**, 3267–3285.
28 O. Tacar, P. Sriamornsak and C. R. Dass, *J. Pharm. Pharmacol.*, 2013, **65**, 157–170.
29 I. Vermes, C. Haanen, H. Steffensnakken and C. Reutelingsperger, *J. Immunol. Methods*, 1995, **184**, 39–51.
30 R. Wilcken, M. O. Zimmermann, A. Lange, A. C. Joerger and F. M. Boeckler, *J. Med. Chem.*, 2013, **56**, 1363–1388.
31 F. Meggio, D. Shugar and L. A. Pinna, *Eur. J. Biochem.*, 1990, **187**, 89–94.
32 R. Battistutta, E. de Moliner, S. Sarno, G. Zanotti and L. A. Pinna, *Protein Sci.*, 2001, **10**, 2200–2206.

33 M. A. Pagano, J. Bain, Z. Kazimierczuk, S. Sarno, M. Ruzzene, G. Di Maira, M. Elliott, A. Orzeszko, G. Cozza, F. Meggio and L. A. Pinna, *Biochem. J.*, 2008, **415**, 353–365.

34 R. Prudent, V. Moucadel, M. Lopez-Ramos, S. Aci, B. Laudet, L. Mouawad, C. Barette, J. Einhorn, C. Einhorn, J.-N. Denis, G. Bisson, F. Schmidt, S. Roy, L. Lafanechere, J.-C. Florent and C. Cochet, *Mol. Cell. Biochem.*, 2008, **316**, 71–85.

35 S. Sarno, E. Papinutto, C. Franchin, J. Bain, M. Elliott, F. Meggio, Z. Kazimierczuk, A. Orzeszko, G. Zanotti, R. Battistutta and L. A. Pinna, *Curr. Top. Med. Chem.*, 2011, **11**, 1340–1351.

36 R. Battistutta, M. Mazzorana, L. Cendron, A. Bortolato, S. Sarno, Z. Kazimierczuk, G. Zanotti, S. Moro and L. A. Pinna, *ChemBioChem*, 2007, **8**, 1804–1809.

37 E. Enkvist, K. Viht, N. Bischoff, J. Vahter, S. Saaver, G. Raidaru, O.-G. Issinger, K. Niefind and A. Uri, *Org. Biomol. Chem.*, 2012, **10**, 8645–8653.

38 T. Fraczyk, K. Kubinski, M. Maslyk, J. Ciesla, U. Hellman, D. Shugar and W. Rode, *Bioorg. Chem.*, 2010, **38**, 124–131.

39 *Schrödinger Suite 2011 (Protein Preparation Wizard, Epik version 2.2, Impact version 5.7, Primer version 3.0) LLC*, New York, 2011.

40 *LigPrep*, Schrödinger, LLC, New York, NY, 2014.

41 R. A. Friesner, R. B. Murphy, M. P. Repasky, L. L. Frye, J. R. Greenwood, T. A. Halgren, P. C. Sanschagrin and D. T. Mainz, *J. Med. Chem.*, 2006, **49**, 6177–6196.

42 T. A. Halgren, R. B. Murphy, R. A. Friesner, H. S. Beard, L. L. Frye, W. T. Pollard and J. L. Banks, *J. Med. Chem.*, 2004, **47**, 1750–1759.

43 R. A. Friesner, J. L. Banks, R. B. Murphy, T. A. Halgren, J. J. Klicic, D. T. Mainz, M. P. Repasky, E. H. Knoll, M. Shelley, J. K. Perry, D. E. Shaw, P. Francis and P. S. Shenkin, *J. Med. Chem.*, 2004, **47**, 1739–1749.

44 I. Ermakova, B. Boldyreff, O. G. Issinger and K. Niefind, *J. Mol. Biol.*, 2003, **330**, 925–934.

45 K. Niefind, C. W. Yde, I. Ermakova and O.-G. Issinger, *J. Mol. Biol.*, 2007, **370**, 427–438.

46 W. Kabsch, *Acta Crystallogr., Sect. D: Biol. Crystallogr.*, 2010, **66**, 125–132.

47 P. Evans, *Acta Crystallogr., Sect. D: Biol. Crystallogr.*, 2006, **62**, 72–82.

48 M. D. Winn, C. C. Ballard, K. D. Cowtan, E. J. Dodson, P. Emsley, P. R. Evans, R. M. Keegan, E. B. Krissinel, A. G. W. Leslie, A. McCoy, S. J. McNicholas, G. N. Murshudov, N. S. Pannu, E. A. Potterton, H. R. Powell, R. J. Read, A. Vagin and K. S. Wilson, *Acta Crystallogr., Sect. D: Biol. Crystallogr.*, 2011, **67**, 235–242.

49 P. D. Adams, P. V. Afonine, G. Bunkoczi, V. B. Chen, I. W. Davis, N. Echols, J. J. Headd, L.-W. Hung, G. J. Kapral, R. W. Grosse-Kunstleve, A. J. McCoy, N. W. Moriarty, R. Oeffner, R. J. Read, D. C. Richardson, J. S. Richardson, T. C. Terwilliger and P. H. Zwart, *Acta Crystallogr., Sect. D: Biol. Crystallogr.*, 2010, **66**, 213–221.

50 A. D. Ferguson, P. R. Sheth, A. D. Basso, S. Paliwal, K. Gray, T. O. Fischmann and H. V. Le, *FEBS Lett.*, 2011, **585**, 104–110.

51 P. Emsley, B. Lohkamp, W. G. Scott and K. Cowtan, *Acta Crystallogr., Sect. D: Biol. Crystallogr.*, 2010, **66**, 486–501.